Charge-coupled-device charge-collection efficiency and the photon-transfer technique

James R. Janesick
Kenneth P. Klaasen
Tom Elliott
Jet Propulsion Laboratory
California Institute of Technology
4800 Oak Grove Drive
Pasadena, California 91109

Abstract. The charge-coupled device has shown unprecedented performance as a photon detector in the areas of spectral response, charge transfer, and readout noise. Recent experience indicates, however, that the full potential for the CCD's charge-collection efficiency (CCE) lies well beyond that realized in currently available devices. In this paper we present a definition of CCE performance and introduce a standard test tool (the photon-transfer technique) for measuring and optimizing this important CCD parameter. We compare CCE characteristics for different types of CCDs, discuss the primary limitations in achieving high CCE performance, and outline the prospects for future improvement.

Subject terms: charge-coupled devices; charge diffusion; x-ray events; frontside illumination; backside illumination.

Optical Engineering 26(10), 972-980 (October 1987).

CONTENTS

1. INTRODUCTION

CCDs in recent years have become the premier detector for use in many spaceborne and ground-based astronomical instruments. They were selected for use in the Hubble Space Telescope Wide Field Planetary Camera (WF/PC), the Galileo Jupiter Orbiter's Solid State Imager (SSI), and many ground-based imaging and spectroscopic applications. Proposed space applications include an x-ray imager on NASA's Advanced X-ray Astronomical Facility (AXAF), a Space Telescope Imaging Spectrometer (SIS), the Solar Optical Telescope (SOT), and the Comet Rendezvous/Asteroid Flyby Imaging Subsystem (CRAF ISS).

Invited Paper CH-102 received April 13, 1987; revised manuscript received May 15, 1987; accepted for publication June 19, 1987; received by Managing Editor July 6, 1987. This paper is a revision of Paper 570-02, presented at the SPIE conference Solid State Imaging Arrays, Aug. 22–23, 1985, San Diego, Calif. The paper presented there appears (unrefereed) in SPIE Proceedings Vol. 570.

The fundamental parameters that ultimately limit CCD performance are (1) read noise, (2) charge-transfer efficiency (CTE), (3) quantum efficiency (QE), and (4) charge-collection efficiency (CCE). At their present stage of development, it is possible to fabricate devices that have low read noise (in the 4 to 15 e^- range), excellent CTE performance (<10 e^- deferred charge), and unsurpassed QE performance over the entire spectral range from 1 to 11,000 Å.[1-3] However, the full potential of charge-collection efficiency lies well beyond that of currently available devices. Optimization of this important parameter represents a new challenge for the CCD manufacturer and user. High CCE performance is required for many applications over all regions of the spectrum to which the CCD is sensitive. In the visible range, for example, CCDs are used in star trackers that demand high sensitivity (charge collection without loss) in conjunction with high geometric accuracy (collection without significant charge diffusion). In the x-ray and EUV regions of the spectrum, applications require confinement of signal charge to a single pixel without loss in order to accurately determine the energy of the incoming photon.

The means of measuring and achieving high CCE performance is the subject of this paper. In Sec. 2 we present a useful definition for CCE performance in terms of parameters that are readily found when testing the CCD. The definition is divided into the two primary factors that are responsible for the degradation of CCE performance, namely, charge loss and charge diffusion. In Sec. 3 we introduce the concept of photon transfer, a technique used as a standard way of measuring CCE characteristics, and develop the theoretical foundations upon which the photon-transfer method is based. We show the strengths and limitations of the photon-transfer technique as it is used in measuring CCE characteristics of the CCD. In Sec. 4 we apply the photon-transfer technique in measuring

CCE performance for frontside- and backside-illuminated CCDs and discuss the primary factors that ultimately limit CCE for each device. Finally, in Sec. 5 we discuss future considerations for further improving CCE for the CCD.

2. CHARGE-COLLECTION EFFICIENCY

CCE is a relatively new CCD performance parameter that has been defined, measured, and optimized at Jet Propulsion Laboratory (JPL) and elsewhere. CCE measures the ability of the CCD to collect all signal charge generated from a single photon event into a single pixel. High CCE performance is especially critical for EUV and soft x-ray applications (e.g., soft x-ray imaging spectrometers), where the ability of the CCD to accurately determine the energy of the photon depends upon collecting the photogenerated charge properly. Experience has shown that complete charge collection requires that two criteria be met: (1) There must be no trapping centers within the CCD to cause signal charge to be lost by recombination, and (2) the charge of an individual photon must be collected within a single pixel and must not be allowed to divide among several pixels. Charge loss causes the photon energy to be underestimated, while charge splitting degrades the precision of charge measurement by requiring the summation of several noisy pixels.

The degree of charge loss and charge splitting depends upon where in the pixel the photon is absorbed. Photons that are absorbed within the frontside depletion region (see Figs. 5 and 8) of a given pixel are typically seen as the ideal event and are called "single-pixel events." Photons absorbed below the depletion region, where the electric field is weaker, create a charge cloud that thermally diffuses outward until it reaches the rapidly changing potential wells at the lower boundary of the pixel array. At that point, the charge cloud may split into two or more packets, which are collected in adjacent pixels. Events of this type are called "split events." Events in which charge is not conserved have been named simply "partial events" and are usually generated in regions deep within the CCD, where loss of carriers through recombination occurs.

From this discussion, a definition for CCE for an individual photon event I can be presented through the formula

$$CCE_I = \frac{\zeta_{pe-I}}{\eta_i P_{se-I}} , \tag{1}$$

where CCE_I represents the fraction of signal electrons, generated by a particular interacting photon I, that is collected in any single affected pixel; ζ_{pe-I} refers to the partial event and represents the number of signal carriers generated by a photon and collected by all pixels (the rest being lost to recombination); P_{se-I} refers to the split event and represents the number of pixels that collect signal electrons generated by a photon; and η_i is defined as the ideal quantum yield, a quantity equal to the total number of electrons generated for an interacting photon of energy E_λ (eV). The ideal quantum yield η_i is directly proportional to the photon energy and is found according to the relationship

$$\eta_i = \frac{E_\lambda}{3.65} \quad (\lambda < 1000\ \text{Å}) . \tag{2}$$

As an example of using Eq. (1), assume that an interacting photon generates 1000 e^- (η_i), with 200 e^- lost to recombination and the 800 e^- remaining (ζ_{pe-I}) split between and collected by two pixels (P_{se-I}). For this event, a CCE_I of 0.4 is calculated no matter in what proportion the 800 e^- are split between the two affected pixels.

To determine the average CCE performance of a CCD for a large number of interacting photons of the same energy, many events are measured for charge loss and splitting and then averaged using the equation

$$CCE = \frac{1}{N\eta_i} \sum_{I=1}^{N} \frac{\zeta_{pe-I}}{P_{se-I}} , \tag{3}$$

where N is the number of photon events sampled.

Equation (3) is used regularly in the laboratory in characterizing the two mechanisms (the partial and split events) responsible for degrading CCE performance of the CCD. However, measuring CCE in the manner described by Eq. (3) requires a considerable amount of data reduction since many events must be integrated. Also, Eq. (3) is usable over only a limited spectral region (typically, $\lambda < 30$ Å) because for longer wavelengths the signal generated by an individual photon becomes too small compared to the CCD read noise floor to reliably resolve the individual event and determine the amount of charge lost and the number of pixels affected.

In this paper we describe another approach to evaluating CCE performance for the CCD that is applicable to all wavelengths of interest. The new technique (discussed in Sec. 3) is based on the formula

$$CCE = \frac{\eta_E}{\eta_i} , \tag{4}$$

where η_E is called the effective quantum yield, a quantity that measures the average number of electrons collected by an affected pixel for an interacting photon of energy E_λ. The effective quantum yield η_E is related to the partial and split events through

$$\eta_E = \frac{\zeta_{pe}}{P_{se}} , \tag{5}$$

where ζ_{pe}/P_{se} is the average value of the term ζ_{pe-I}/P_{se-I}.

3. PHOTON-TRANSFER TECHNIQUE

The ideal CCD, which does not generate split or partial events but exhibits perfect CCE performance, will deliver an effective quantum yield equal to the ideal quantum yield (i.e., $\eta_E = \eta_i$). Today's CCDs are rapidly progressing toward this ultimate goal; however, very strict conditions are placed on the CCD in obtaining such performance, as we shall see in Sec. 4. Because of the various CCD technologies and manufacturers involved in fabricating CCDs, a standard "test tool" for evaluating CCE performance over a very large spectral range is required.

In this section we discuss the technique of photon transfer, a test tool that was used in the past to evaluate CCD performance characteristics in absolute units.[1] It was realized only recently that the photon-transfer technique also can be applied as a standard method for evaluating the CCE performance of a CCD. In the discussion that follows, we first develop the equations necessary to describe the technique,

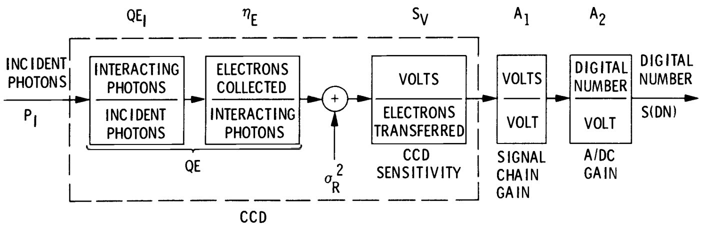

Fig. 1. Schematic showing individual transfer functions of an ideal CCD camera.

assuming that we have an ideal CCD camera with no partial or split event generation. We show that the ideal quantum yield η_i can be determined through the photon-transfer approach. We next examine a typical CCD camera, which includes partial and split event generation, and show that the photon-transfer technique gives a reasonable approximation for the effective quantum yield η_E, defined in Eq. (5), which in turn is used to calculate the CCE performance of the CCD [Eq. (4)], at least in a relative sense.

3.1. Ideal CCD camera

Figure 1 is a schematic representation of the overall transfer function of an ideal CCD camera. The camera can be described in terms of five transfer functions, three that are related to the CCD and two that are related to the external CCD signal processing circuitry. The input to the camera is given in units of incident photons, and the final output of the camera is achieved by encoding each pixel's signal into a digital number (DN), typically using 12 to 16 bits. The output signal S (DN) resulting from a given exposure of the CCD camera shown in Fig. 1 is given by

$$S\,(DN) = PQE_I \eta_i S_V A_1 A_2 \ , \tag{6}$$

where S (DN) represents the average signal (DN) over all affected pixels, P is the mean number of incident photons per pixel on the CCD, QE_I is defined as the interacting quantum efficiency (interacting photons/incident photons), η_i is the ideal quantum yield defined by Eq. (2), S_V is the sensitivity of the CCD on-chip circuitry (V/e^-), A_1 is the electronic gain of the camera (V/V), and A_2 is the transfer function of the analog-to-digital converter (DN/V).

The quantities QE_I and η_i are related through

$$QE = \eta_i QE_I \ , \tag{7}$$

where QE is the average quantum efficiency (electrons collected/incident photon).

To convert the output signal S (DN) into fundamental physical units, it is necessary to find the appropriate factors to convert DN units into either interacting photons or signal electrons. The constants that do this conversion are defined by the equations

$$K = (S_V A_1 A_2)^{-1} \ , \tag{8}$$

$$J = (\eta_i S_V A_1 A_2)^{-1} \ , \tag{9}$$

where the units of K and J are e^-/DN and interacting photons/DN, respectively. Note that Eqs. (8) and (9) are related through η_i by

$$\eta_i = \frac{K}{J} \ . \tag{10}$$

It is possible to determine the factors K and J by measuring each transfer function in Fig. 1 separately and then combining these results as in Eqs. (8) and (9). However, because of the uncertainty in a number of parameters of the CCD (which prevents us from knowing QE_I, η_i, and S_V independently), we cannot in practice directly determine K or J to any great accuracy. Instead, we have developed a simple technique that requires no knowledge of the individual transfer functions to determine the factors K and J.

3.2. Evaluation of constant K

For the CCD stimulated with photons that generate only one electron-hole (e-h) pair for each interaction (i.e., $\eta_i = 1$; $\lambda > 3000$ Å), Eq. (6) reduces to the form

$$S\,(DN) = PIK^{-1} \ , \tag{11}$$

where $PI = PQE_I$ represents the number of interacting photons per pixel.

The constant K can be determined by relating the output signal S (DN) to its variance, σ_S^2 (DN). The variance σ_S^2 (DN) of Eq. (11) is found using the propagation of errors, which yields the following equation for the ideal CCD (i.e., perfect charge collection and charge transfer):

$$\sigma_S^2\,(DN) = \left[\frac{\partial S\,(DN)}{\partial PI}\right]^2 \sigma_{PI}^2 + \left[\frac{\partial S\,(DN)}{\partial K}\right]^2 \sigma_K^2 + \sigma_R^2\,(DN) \ , \tag{12}$$

where we have added in quadrature the read noise floor variance σ_R^2 (DN) [see Fig. 1; $\sigma_R^2\,(DN) = \sigma_R^2\,(e^-)\,K^{-2}$].

Performing the required differentiation on Eq. (12) and assuming that the constant K has negligible variance (i.e., $\sigma_K^2 = 0$), we find the following expression for the variance in S (DN):

$$\sigma_S^2\,(DN) = \left(\frac{\sigma_{PI}}{K}\right)^2 + \sigma_R^2\,(DN) \ . \tag{13}$$

Since $\sigma_{PI}^2 = PI$ because of photon statistics, the following equation for the constant K in terms of S (DN) and σ_S^2 (DN) results:

$$K = \frac{S\,(DN)}{\sigma_S^2\,(DN) - \sigma_R^2\,(DN)} \quad (\lambda > 3000\ \text{Å}) \ . \tag{14}$$

Equation (14) is a useful expression and can be used, with no further calibration, to convert output measurements in DN directly into units of electrons.

3.3. Evaluation of constant J

For wavelengths longer than 3000 Å, the constants K and J are equivalent [Eq. (10), $\eta_i = 1$]. However, as we move into the UV, EUV, and x-ray regions of the spectrum, multiple e-h pairs are generated by each interacting photon, resulting in $\eta_i > 1$ and a decrease in the value J. For these conditions, the constant J also can be found by relating the output signal S (DN), given by Eq. (6), to its variance σ_S^2 (DN). Through propagation of errors, the variance in the signal for the ideal CCD can be expressed by

$$\sigma_S^2(\mathrm{DN}) = \left[\frac{\partial S(\mathrm{DN})}{\partial \mathrm{PI}}\right]^2 \sigma_{\mathrm{PI}}^2 + \left[\frac{\partial S(\mathrm{DN})}{\partial \eta_i}\right]^2 \sigma_{\eta_i}^2 + \left[\frac{\partial S(\mathrm{DN})}{\partial K}\right]^2 \sigma_K^2 + \sigma_R^2(\mathrm{DN}) \ . \quad (15)$$

Differentiating Eq. (15) and assuming that the quantum yield η_i has negligible variance (i.e., no partial or split event; $\sigma_{\eta_i}^2 = 0$), we find

$$J = \frac{S(\mathrm{DN})}{\sigma_S^2(\mathrm{DN}) - \sigma_R^2(\mathrm{DN})} \quad (\lambda < 3000 \text{ Å}) \ . \quad (16)$$

Equations (14) and (16) form the basis for the photon-transfer technique. By simply measuring the mean signal and its variance for both visible photons and photons at any other specific wavelength of illumination, we can determine the values K and J. Once the constants K and J are known, the ideal quantum yield for photons at the wavelength under consideration can be calculated through Eq. (10).

3.4. Partial and split events included

Up to this point, we have assumed no partial or split event generation within the CCD (i.e., $\eta_E = \eta_i$). We now show that the ratio K/J with partial and split events included gives an upper limit for the effective quantum yield η_E, which in turn gives an upper limit for CCE performance for the CCD as defined by Eq. (4). We also show that as the number of partial and split events within the CCD decreases, the ratio K/J approaches the real value of η_E and in the limit η_E equals η_i, when perfect CCE is achieved.

To analytically solve for the constant J under these conditions, we must give Eq. (6) a new form so that the variances of the partial and split events are included when the overall variance of the signal is calculated. Such an equation for the average signal in any given pixel can be written in the form

$$S(\mathrm{DN}) = \mathrm{PI}\eta_i M \left(\frac{\zeta_{pe}}{P_{se}\eta_i}\right) K^{-1} \ , \quad (17)$$

where M is the average number of interacting photons per pixel.

It is informative to compare the behavior of the signal given by Eq. (17) to the signal given in Eq. (6) for the ideal CCD camera without partial or split events. The signal described in Eq. (6) is proportional to η_i and is not influenced by CCE characteristics since CCE is assumed to be perfect. In the case of Eq. (17), we find that the signal is proportional to (ζ_{pe}/P_{se}) when the number of interacting photons per pixel is small (i.e., $M \approx 1$) and interactions are not adjacent to each other in the CCD array. In this case, the amount of signal measured is dependent on both partial and split event behavior. However, when the number of interacting photons per pixel is large (i.e., $M \approx P_{se}$), the signal is dependent only on the partial event [i.e., $S(\mathrm{DN}) = \mathrm{PI}\zeta_{pe}K^{-1}$] and the effects of the split event are averaged out.

It can be shown, again using propagation of errors, that the signal S (DN), given by Eq. (17), and its variance σ_S^2 (DN) are related to the effective quantum yield by

$$\eta_E = K\left[\frac{S(\mathrm{DN})}{\sigma_S^2(\mathrm{DN}) - \sigma_R^2(\mathrm{DN})}\left(P_{se} + \frac{2\sigma_P^2}{P_{se}} + \frac{P_{se}\sigma_\zeta^2}{\zeta_{pe}^2}\right)\right]^{-1} \ , \quad (18)$$

where σ_P^2 is the event-to-event variance in the number of pixels that collect signal electrons per interacting photon and σ_ζ^2 is the event-to-event variance for the total number of electrons collected. Here, we have assumed that the average of ζ_{pe-I}/P_{se-I} is equal to the average of ζ_{pe-I} divided by the average of P_{se-I}, which becomes nearly correct for large numbers of photon events.

Equation (18) also can be written in the form

$$\eta_E = \frac{K}{J\epsilon} \ , \quad (19)$$

where ϵ is $P_{se} + 2(\sigma_P^2/P_{se}) + P_{se}(\sigma_\zeta^2/\sigma_{pe}^2)$ and K and J are as defined in Eqs. (14) and (16), which we normally measure using the photon-transfer technique.

The true value of the effective quantum yield η_E given by Eq. (19) is less than K/J by the factor ϵ^{-1}. As the number of partial and split events decreases, the accuracy of K/J improves and in the limit is exact when $\epsilon = 1$ (i.e., $\eta_E = \eta_i$). Therefore, when measuring the effective quantum yield using the photon-transfer technique in the presence of partial and split events, the ratio K/J gives an upper limit for η_E. For example, for the Texas Instruments (TI) 3PCCD (a CCD type discussed in Sec. 4), we find experimentally that for individual 5.9 keV (Fe^{55}) photon events, one out of 11 events splits between 2 pixels, with only a few partial events observed. For this CCD we calculate an average P_{se} of 1.09 pixels with variances $\sigma_P^2 = 0.166$ and $\sigma_\zeta^2 \approx 0$. Assuming these values, we find that $\epsilon^{-1} = 0.72$. Therefore, the true value of η_E is actually smaller by 0.72 than the value of η_E measured using the photon-transfer method (i.e., K/J).

Even though the ratio K/J does not give an exact value for the effective quantum yield, this quantity still is useful in evaluating and optimizing CCE performance of the CCD, as we shall see in Sec. 4. Therefore, unless otherwise indicated, we use the ratio K/J as found through the photon-transfer method as our standard measuring tool in comparing η_E and CCE performance for different CCDs under different operating conditions, while keeping in mind that the absolute values of these quantities are lower (by ϵ^{-1}).

3.5. Photon-transfer curve

The constants K and J can be found either graphically or directly through Eqs. (14) and (16). We examine the graphical approach first because the method gives insight into the mechanics of the photon-transfer technique.

The constants K and J can be found graphically by plotting a curve (called the "photon-transfer curve") of noise σ_S (DN) as a function of signal S (DN), typically for a 20×20 pixel array on the CCD. One such photon-transfer curve is shown in Fig. 2. For this curve we use 7000 Å illumination, which guarantees that $\eta_E = \eta_i = 1$ and therefore can be used in finding the constant K. The abscissa, S (DN), is the average signal level of the 400 pixels with the array uniformly illuminated at some level. (Here, we assume that electrical offset and

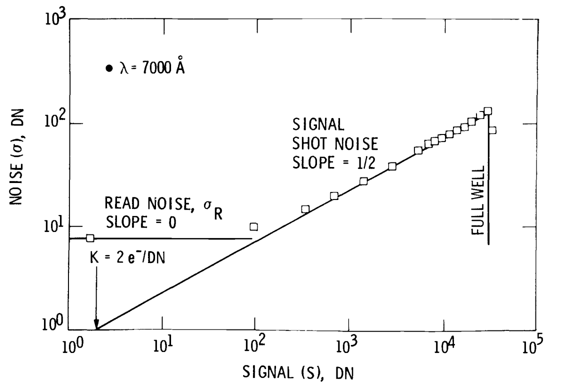

Fig. 2. Photon-transfer curve using 7000 Å illumination ($\eta_i = 1$).

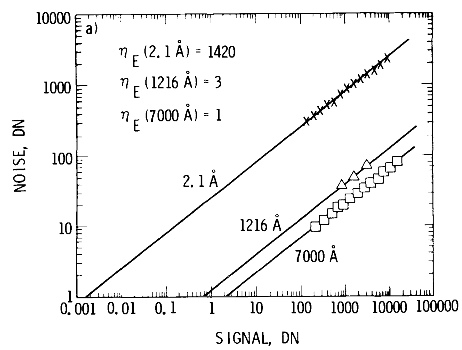

Fig. 3. Photon-transfer curves taken at three photon energies, each yielding a different effective quantum yield.

dark current were subtracted from the data before the signal level was determined.) The ordinate, σ_S (DN), is the standard deviation of the signal of those 400 pixels at each exposure. The standard deviation is found after the CCD pixel-to-pixel nonuniformity has been removed. This can be accomplished by differencing (pixel by pixel) two frames taken at the same light level, calculating the standard deviation of the resultant difference, and dividing by 2, which yields the desired σ_S (DN).

The read noise σ_R (DN), indicated in Fig. 2, represents the intrinsic noise associated with the readout circuitry, i.e., the CCD on-chip amplifier and any other noise sources that are independent of the signal level. As the signal is increased, the noise eventually becomes dominated by the shot noise of the signal and is characterized by a line of slope 1/2. From Eq. (14) we note that the intersection of the slope 1/2 line of the signal axis [i.e., σ_S (DN) $= 1$] represents the desired conversion constant K.

The same graphical approach can be used in determining the constant J when $\eta_i > 1$ [Eq. (16)]. For example, in Fig. 3 we show three photon-transfer curves (taken with the same CCD camera and CCD) generated from flat fields at wavelengths of 7000 Å, 1216 Å, and 2.1 Å. The corresponding intersections on the signal axis at each of these wavelengths are 2.3, 0.77, and 1.62×10^{-3}. Since $\eta_E = \eta_i = 1$ for 7000 Å illumination, the signal at σ_S (DN) $= 1$ for this photon-transfer curve represents the value of constant K (i.e., $K = 2.3\ e^-/DN$). The other two intersections, for the wavelengths 1216 Å and 2.1. Å, represent values for J that can be used in conjunction with K to find η_E ($= K/J$), yielding an

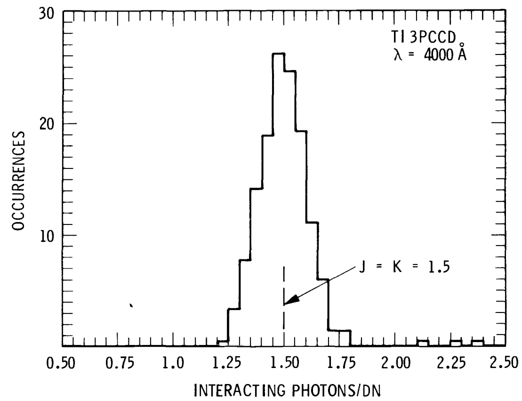

Fig. 4. Photon-transfer histogram using 4000 Å illumination ($\eta_i = 1$).

average of 3 e^- and 1420 e^- per affected pixel per interacting photon, respectively.

In the case of 2.1 Å ($E_\lambda = 5.9$ keV; $\eta_i = 1610\ e^-$), the photon-transfer technique yields a K/J of 1420 e^-. An actual η_E of 1215 e^- is readily determined by measuring individual photon events [Eq. (5)], which gives a value for ϵ^{-1} in Eq. (19) of 0.85. From Eq. (4), an upper limit of 0.88 for CCE performance is calculated using K/J found from the photon-transfer curve, while a true CCE of 0.75 is calculated using individual photon events. This level of CCE performance is quite good by today's CCD standards.

3.6. Photon-transfer histogram

The accuracy of determining K and J can be improved by using Eqs. (14) and (16) directly (as opposed to the graphical approach used in Sec. 3.5). The signal S (DN) and the noise σ_S (DN) are found from the CCD in the same manner as for the photon-transfer curve discussed above. The read noise σ_R (DN) is found from a dark image. After applying these formulas to many different 20×20 pixel subarrays across the sensor, the resulting values of K (or J) are compiled into a form we call a "photon-transfer histogram." An example histogram using 4000 Å illumination is shown in Fig. 4. It produces a very accurate value of $K = 1.5\ e^-/DN$. Using many 20×20 pixel subarrays allows elimination of those regions on the device that contain blemish artifacts, which give erroneous values for K. Areas that are not well behaved can be easily recognized as data points outside the main histogram, as Fig. 4 shows. A similar histogram also can be generated over the entire CCD array for η_E ($= K/J$) at a specific wavelength of interest. This type of histogram is quite valuable in characterizing the variability of CCE performance across the array of the CCD. In Sec. 4 we depict the use of histograms of η_E under different operating conditions of the CCD.

4. PHOTON-TRANSFER USE

In this section we apply the photon-transfer technique to measuring CCE performance for two different types of CCDs, namely, the thick TI frontside-illuminated virtual-phase CCD (TI VPCCD) and the thin TI backside-illuminated three-phase CCD (TI 3PCCD). These devices are discussed in considerable detail elsewhere.[1-3] The CCDs used in tests discussed here have approximately the same read noise floor, charge-transfer efficiency, and quantum efficiency performance for

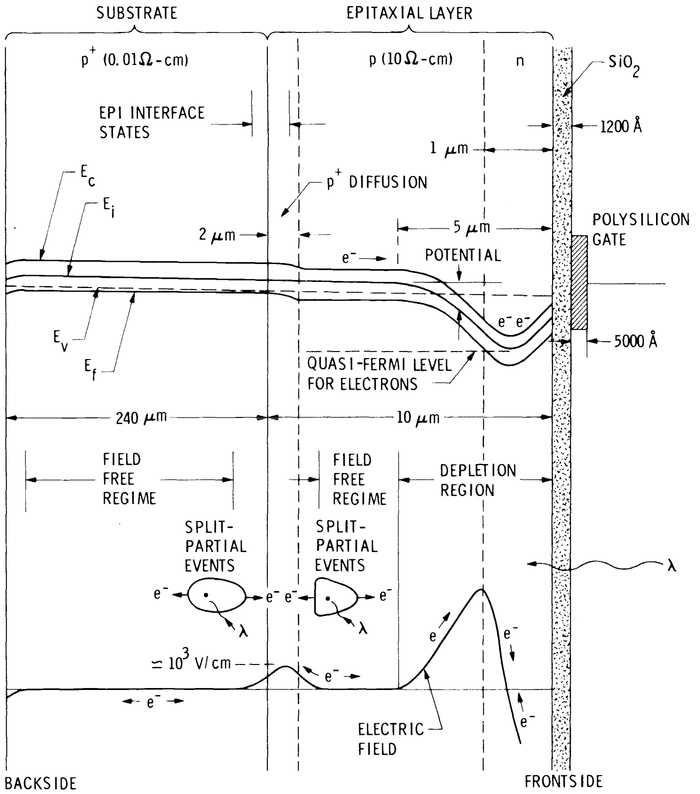

Fig. 5. Cross section of a thick frontside-illuminated CCD, showing energy band structure and locations at which partial and split event generation occurs.

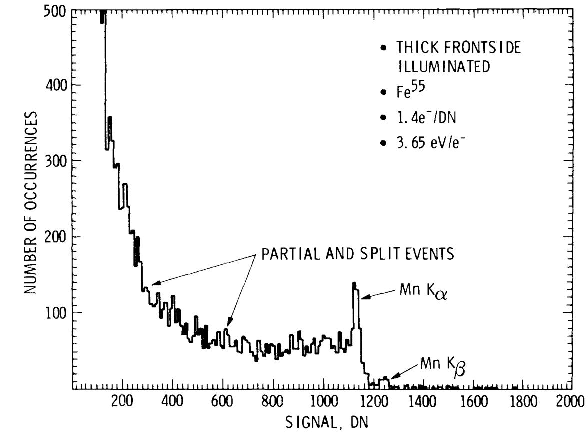

Fig. 6. Fe^{55} x-ray histogram for a thick frontside-illuminated CCD, showing numerous partial and split events.

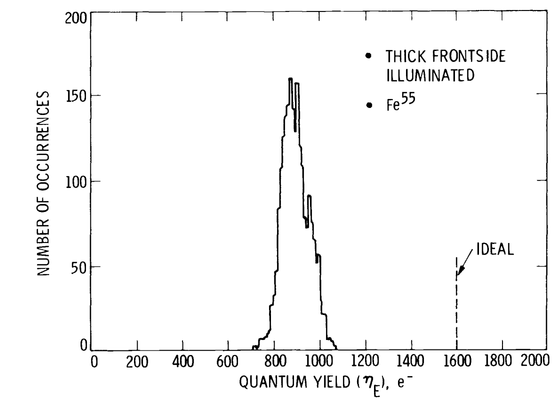

Fig. 7. Histogram of effective quantum yield η_E for a thick frontside-illuminated CCD.

the wavelengths used. However, we show that CCE performance for the two CCDs is significantly different owing to the number of partial and split events generated in each device.

4.1. Frontside illumination (TI VPCCD)

In general, we find numerous partial and split events for the thick frontside-illuminated epitaxial CCD. Such a device is schematically represented in Fig. 5, which shows the primary regions within the CCD that are responsible for generating split and partial events. Photons that interact in the substrate region produce a charge cloud that has a high probability of recombination owing to the high concentration of holes in this region and the existence of bulk interface states at the epitaxial interface. The physical size of the charge cloud also is likely to span the boundary between adjacent pixels. Such interactions tend to result in split and partial events. Photons that interact between the epitaxial interface and frontside depletion region also generate split events due to charge diffusion in the field-free region and partial events due to signal charge diffusing through the weak field produced by the p^+ diffusion into the bulk traps at the epitaxial interface (see Fig. 5).

Figure 6 shows the response of the TI VPCCD uniformly illuminated by an Fe^{55} x-ray source with a mean flux of approximately 1 x ray per 500 pixels. The DN of each pixel on the CCD containing signal charge is measured and appropriately binned in histogram form. Ideally, the response of Fig. 6 should show only two prominent peaks, located at 1150 DN (1610 e^-) and 1270 DN (1780 e^-) due to the Mn-K_α and Mn-K_β x rays generated by the F^{55} source. The events with signals below these two lines are the result of split and partial events and constitute the majority of the events observed.

Figure 7 shows a histogram of effective quantum yield η_E calculated by the photon-transfer method for the same TI VPCCD used in generating the histogram shown in Fig. 6. The histogram is generated by uniformly stimulating the CCD with a mean flux of about 5 x rays per pixel (Fe^{55}) and calculating η_E for several different 40×40 pixel subarrays across the sensor. We find from Fig. 7 an average effective quantum yield of 900 e^-/pixel/interacting photon, which is significantly less than the ideal quantum yield η_i of 1610 e^-. The relative CCE performance for this device is readily calculated to be 0.56 using Eq. (4).

4.2. Backside illumination (TI 3PCCD)

For the backside-illuminated CCD, in which the substrate and epitaxial interface are removed (Fig. 8), the number of partial and split events is significantly reduced. It has been demonstrated that an internal QE of 100% can be achieved (i.e., $\zeta_{pe}/\eta_i = 1$) for the CCD that is properly thinned and backside treated.[4–6] The main factor that determines CCE performance for the backside-illuminated CCD is the split event.

To minimize the number of split events for the backside-illuminated CCD, it is important that an electric field of greater than 10^5 V/cm be provided throughout the entire photosensitive depth of the CCD. Regions in which the field

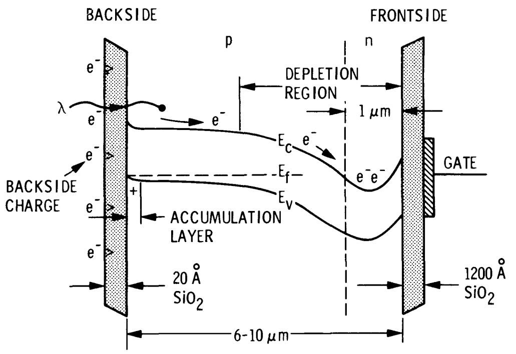

Fig. 8. Cross section of a thin backside-illuminated CCD that is backside charged, showing energy band structure.

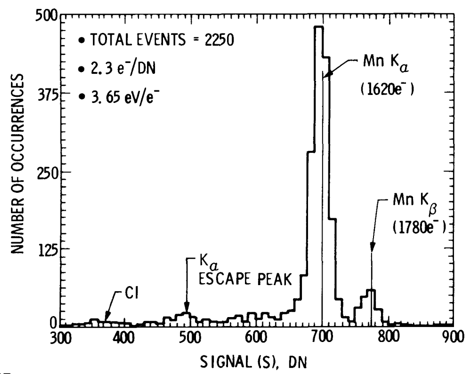

Fig. 9. Fe^{55} x-ray histogram for a thin backside-illuminated CCD, showing very few partial and split events.

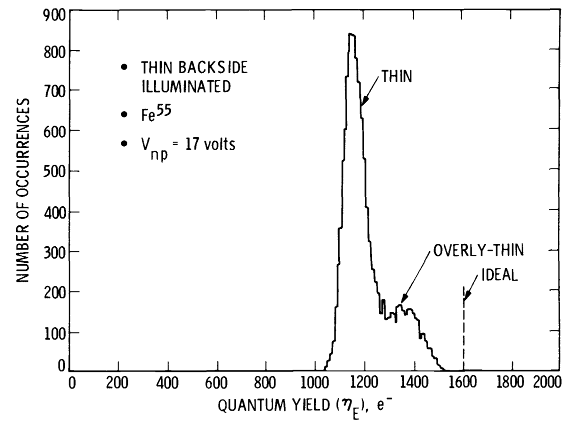

Fig. 10. Histogram of effective quantum yield η_E for a thin backside-illuminated CCD.

strength is lower permit the charge cloud to diffuse to a large size, making it likely to overlap more than one pixel and split. For the TI 3PCCD, it has been demonstrated that a high field condition throughout a 7 μm region can be achieved using backside charging or a flash gate and proper bias conditions across the n-channel and substrate (Fig. 8).

Figure 9 shows a histogram response to Fe^{55} x rays of a TI 3PCCD that is properly thinned (i.e., thinned to the frontside depletion edge) and backside treated. Comparing Figs. 6 and 9, we note that the number of partial and split events is significantly less for the backside-illuminated CCD than for the frontside-illuminated CCD.

Figure 10 shows a TI 3PCCD histogram of the effective quantum yield for Fe^{55} x rays, generated using the photon-transfer method. We note from this figure that two regions on the CCD (labeled thin and overly thin) produce different quantum yields. The overly thin region is slightly thinner than the thin region and represents where the frontside depletion edge has reached the backside. The thicker region exhibits degraded performance because of a larger field-free region, which causes more charge splitting due to diffusion and results in a lower effective quantum yield. The variability of quantum yield across the CCD membrane can be seen more clearly in Fig. 11, in which η_E is displayed in image format as a result of calculating K/J for 160,000 subarrays across the CCD. Figure 12 is an expanded view of the upper right-hand corner of Fig. 11, and Fig. 13 is a corresponding printout of η_E. It is seen from Figs. 12 and 13 that the quantum yield for this device varies considerably from 1400 e^- in the corners (white regions) to 1200 e^- in the middle (black regions). The differences in η_E are the result of thinning nonuniformities, where the four corners are physically thinner than the middle of the array because of the thinning method employed.

Figure 14 shows η_E histograms for a different TI 3PCCD biased with different frontside depletion voltages (V_{np}) across the n-channel and p-substrate.[5] The distance that the edge of the depletion region extends into the substrate is proportional to $V_{np}^{1/2}$ and therefore influences the field-free region of the CCD. From these figures we see that the effective quantum yield decreases significantly as V_{np} is lowered due to an increase in field-free material, which causes more diffusion and charge splitting. Figure 15 shows an η_E image over the CCD array for $V_{np} = 7$ V; note two distinct areas that correspond to the thin and overly thin regions indicated in Fig. 14(b).

The last η_E histogram, shown in Fig. 16, is similar to that of Fig. 10 but has an elevated frontside depletion voltage of $V_{np} = 27$ V and represents the best CCE performance achieved for the TI 3PCCD. For the overly thin region, an average quantum yield of 1420 e^- was measured, which yields a relative CCD = 0.88. We believe that this limit in CCE performance for the TI 3PCCD is due primarily to two factors: First, the initial cloud diameter size for a 5.9 keV photon event is significant (cloud diameter ≈ 0.6 μm); therefore, charge splitting between the TI 3PCCD's 15 μm pixels occurs even if there is no field-free material. Second, it is known that a field-free region exists beneath the channel stop regions, which allows charge diffusion and charge splitting to occur. Both of these effects are discussed in detail in Ref. 7, where it is shown that increasing the size of the pixel improves the CCE performance further because of these two factors.

5. FUTURE IMPROVEMENTS IN CCE

At this time in the development of the CCD, the backside-illuminated device is superior to the frontside-illuminated device in achieving high CCE performance. This is because the backside-illuminated CCD allows field control over most of the photosensitve volume and elimination of neutral bulk and trapping centers at which photogenerated charge can diffuse and recombine to produce partial and split events.

Improvements in CCE for the backside-illuminated CCD will be made principally in two areas. The first area for

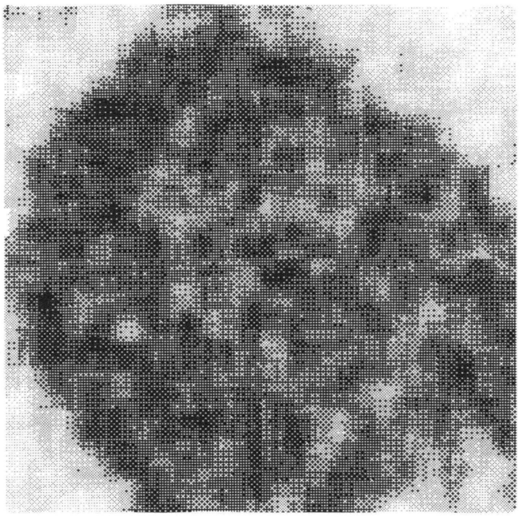

Fig. 11. Pictorial display of the effective quantum yield for a thin backside-illuminated CCD, showing regions of different thickness.

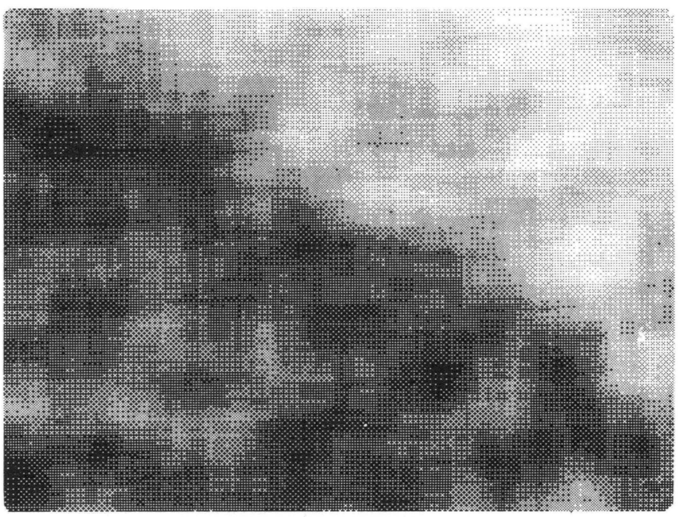

Fig. 12. Magnified view of upper right-hand corner of Fig. 11.

1248	1251	1323	1346	1382	1369	1348	1440	1420	1478	1526	1434	1415
1273	1246	1261	1344	1354	1314	1339	1420	1420	1441	1471	1475	1437
1192	1157	1230	1248	1255	1321	1344	1303	1413	1375	1391	1489	1431
1058	1117	1149	1139	1232	1416	1374	1293	1337	1342	1462	1500	1428
1131	1118	1141	1129	1280	1270	1328	1339	1402	1413	1456	1391	1358
1099	1127	1183	1154	1241	1185	1270	1337	1399	1326	1332	1373	1411
1157	1154	1207	1142	1171	1116	1116	1186	1231	1280	1324	1461	1441
1199	1221	1217	1193	1151	1168	1171	1142	1180	1282	1379	1461	1369
1130	1130	1207	1172	1185	1191	1116	1152	1202	1146	1236	1318	1319
1166	1167	1198	1204	1220	1188	1121	1171	1117	1131	1157	1202	1325
1231	1203	1170	1135	1207	1207	1134	1121	1046	1216	1171	1159	1316
1202	1221	1279	1241	1264	1129	1094	1157	1204	1239	1175	1136	1187
1135	1063	1147	1189	1203	1082	1153	1175	1186	1146	1116	1157	1142

CORNER QUANTUM YIELDS, η_E

Fig. 13. Printout representing effective quantum yield of the region shown in Fig. 12.

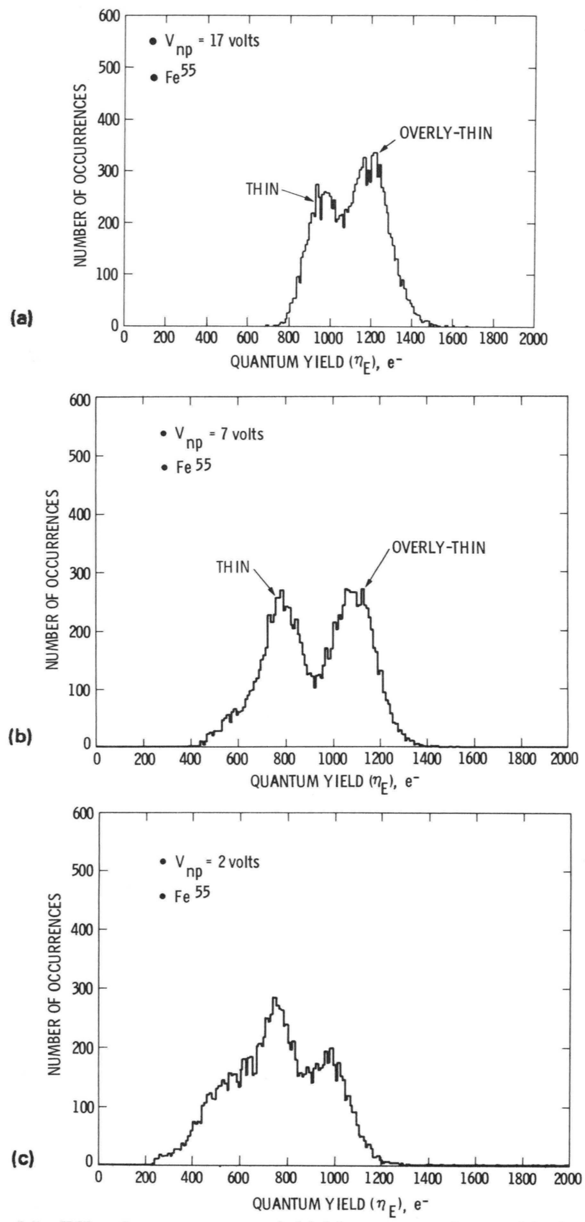

Fig. 14. Effective quantum yield histograms for a thin backside-illuminated CCD using frontside depletion voltages of (a) 17 V, (b) 7 V, and (c) 2 V.

improvement will come from depleting the entire photosensitive volume of the CCD. Although complete depletion already has been demonstrated for the TI 3PCCD in certain regions on the array, depletion extends only a maximum of 7 μm. Therefore, high energy efficiency and cosmic ray background rejection characteristics are still poor for this sensor. Increasing the thickness of the CCD and depleting it fully through deep depletion technology (high resistivity silicon) in conjunction with backside treatment should yield both high CCE and high energy sensitivity for the CCD. Work at several CCD manufacturers has been initiated to accomplish this goal.

Second, larger pixels ($\sim$30 μm) would increase CCE performance further by making a larger "target" for the incoming photon and reducing the effects of the initial event cloud diameter. In addition, a smaller fraction of the pixel is devoted to "overhead" functions such as the channel stop regions, which tend to increase the number of split events by diffusion.

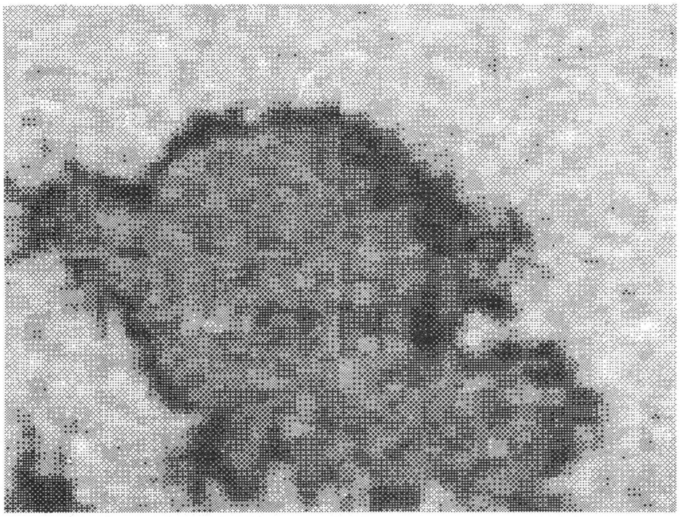

Fig. 15. An effective quantum yield image for the histogram of Fig. 14(b).

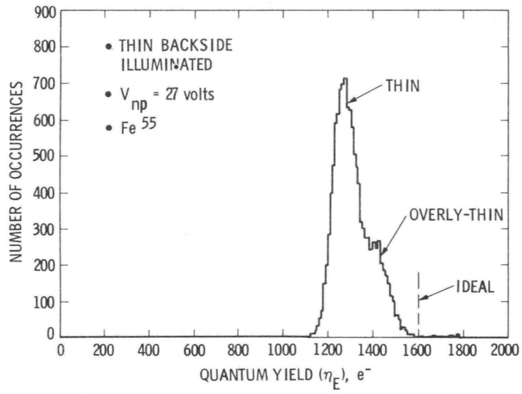

Fig. 16. Histogram of best effective quantum yield for the TI 3PCCD, using a frontside voltage of 27 V.

6. ACKNOWLEDGMENTS

The authors acknowledge many rewarding conversations on the subject of CCE with Morley Blouke (father of the TI 3PCCD), Taher Daud, Andy Collins, Dave Campbell, James DeWitt, Arsham Dingizian, and James McCarthy. We also thank Deborah Durham for reviewing this paper. The research described was carried out by the Jet Propulsion Laboratory, California Institute of Technology, under contract with the National Aeronautics and Space Administration.

7. REFERENCES

1. J. R. Janesick, T. Elliott, S. Collins, M. M. Blouke, and J. Freeman, "Scientific charge-coupled devices," Opt. Eng. 26(8), 692–714 (1987).
2. M. M. Blouke, J. R. Janesick, T. Elliott, J. E. Hall, M. W. Cowens, and P. J. May, "Current status of 800×800 charge-coupled-device imager sensor," Opt. Eng. 26(9), in press (1987).
3. J. R. Janesick, J. Hynecek, and M. M. Blouke, "Virtual phase imager for Galileo," in *Solid State Imagers for Astronomy,* J. C. Geary and D. W. Latham, ed., Proc. SPIE 290, 165–173 (1981).
4. J. Janesick, T. Elliott, T. Daud, J. McCarthy, and M. Blouke, "Backside charging of the CCD," in *Solid State Imaging Arrays,* K. N. Prettyjohns and E. L. Dereniak, eds., Proc. SPIE 570, 46–79 (1985).
5. J. Janesick, T. Elliott, T. Daud, and D. Campbell, "The CCD flash gate," in *Instrumentation in Astronomy VI,* D. L. Crawford, ed., Proc. SPIE 627, 543–582 (1986).
6. J. Janesick, D. Campbell, T. Elliott, T. Daud, and P. Ottley, "Flash technology for CCD imaging in the UV," in *Ultraviolet Technology,* R. Huffman, ed., Proc. SPIE 687, 36–55 (1986).
7. J. Janesick, T. Elliott, J. McCarthy, H. Marsh, and S. Collins, "Present and future CCDs for UV and x-ray scientific measurements," IEEE Trans. Nuc. Sci. NS-32 (1), 409–416 (1985).

James R. Janesick: Biography and photograph appear with the Guest Editorial in this issue.

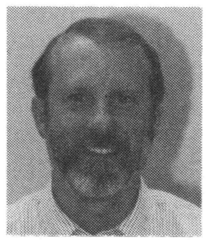

Kenneth P. Klaasen is the supervisor of the Photoscience Group at JPL. He received his BS degree in physics from Calvin College, Grand Rapids, Mich., and his MS in aerospace engineering from the University of Michigan in 1969. He has been involved in many solar system exploration missions, including Mariner 10, the Viking Orbiter, and currently the Galileo mission to Jupiter. He has served as the experiment representative for the imaging experiments on these missions and is currently a member of the Galileo Imaging Science Team. His primary responsibilities have included imaging system calibration, experiment planning, and mission operations. He has published papers on the rotation period of Mercury, Venus atmospheric dynamics, and the photometry of Mercury, Mars, and the Martian moons, Phobos and Deimos, as well as several on various spacecraft imaging instruments and experiments.

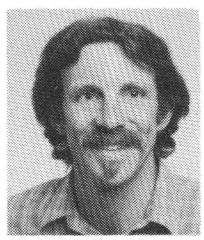

Stythe T. Elliott was born in Van Nuys, California. He received his BA degree in geography from the California State University at Northridge. He joined the Jet Propulsion Laboratory in 1979 and is presently working on developing charge-coupled devices for NASA space imaging systems. He received a NASA Achievement Award in 1986. He is currently involved with the development of CCDs used in the wide field/planetary Hubble Space Telescope camera.